Thermalisation time of electron swarms in xenon for uniform electric fields

G J Boyle[1,4], M J E Casey[1], D G Cocks[2], R D White[1] and R J Carman[3]

[1]College of Science, Technology and Engineering, James Cook University, Townsville, Australia
[2]Research School of Physics and Engineering, Australian National University, Canberra, Australia
[3]Department of Physics and Astronomy, Macquarie University, Sydney, Australia
[4]Present address: DESY, Hamburg, Germany

E-mail: gregory.boyle@my.jcu.edu.au and robert.carman@mq.edu.au

Received xxxxxx
Accepted for publication xxxxxx
Published xxxxxx

Abstract

We have calculated the thermalisation time for an electron swarm in gaseous xenon using a multi-term time-dependent Boltzmann equation (BE), for a range of instantaneously applied reduced electric fields 1Td<E/N<1000Td. Starting from a Maxwellian electron energy distribution function (EEDF) at room temperature for a given E/N, the time-evolution of the EEDF and associated electron swarm parameters (drift velocity W_e, mean energy $\langle\varepsilon\rangle$, ionisation coefficient k_i, excitation coefficient k_{ex}) are followed as they converge to steady-state values. For all values of E/N considered, the individual swarm parameters are found to converge at different rates. For E/N>5Td, they converge in order W_e (fastest), $\langle\varepsilon\rangle$, k_{ex}, and k_i (slowest). The time taken for the slowest swarm parameter to converge to an acceptable level (e.g. to within 90% of its steady-state value) is used universally as the benchmark for evaluating the thermalisation time τ_{th}. This time is found to be strongly dependent on the value of the reduced electric field E/N, dropping by almost 5 orders of magnitude for increasing E/N fields 1Td<E/N<1000Td. As a key outcome from this work, the calculated thermalisation times $\tau_{th}.p$ are expressed as a general formula, as a function of both the reduced electric field E/N and a user defined convergence level between 80-99%. We also show that ballpark estimates of thermalisation times, based on the inverse of the collision frequency for energy dissipation $1/\nu_e(\varepsilon)$ at typical average electron energies, are likely to be unreliable if applied to the heating phase. We also undertake a brief analysis of the cooling phase when the electric field is instantaneously removed from the plasma (i.e. field-free) after it evolves to steady-state conditions during the previous heating phase. Finally, we compare calculated thermalisation times with the typical risetimes of the voltage pulse waveforms for several experimental “nanosecond” pulse excited plasma discharge devices.

Keywords: plasma, electron, thermalisation, xenon, multi-term Boltzmann equation, nanosecond discharge

1. Introduction

For the broad range of weakly-ionised collision-dominated medium- to high-pressure plasmas (p=0.01-5bar) operating in the non local thermodynamic equilibrium (non-LTE) regime, the time taken for an electron swarm to reach a state of equilibrium (or thermalise) with an instantaneously applied constant electric field in the range E/N=10-300Td is very short, typically less than 10^{-9}s [1] [2] [3] [4]. Thus, to undertake time-dependent numerical modelling of these non-LTE plasmas driven by relatively slow time-varying voltage waveforms ($\tau>>10^{-9}$s), a steady-state Boltzmann code is usually sufficient to deduce the electron energy distribution function (EEDF) and the requisite electron swarm parameters as a function of the reduced field E/N [2] [5] [6] [7]. Recently, however, plasmas driven by fast transient voltage pulses (e.g. risetimes >100V.ns^{-1}, 1-10ns duration) are being rapidly developed, as reviewed in 2017 in [8]. It is not yet clear whether the EEDFs in these new fast transient plasmas deviate significantly from "thermalised" due to the rapid change of E/N in time. If the EEDFs are not fully thermalised during this heating phase, numerical modelling must be undertaken instead using a fully time-dependent Boltzmann code which is significantly more computationally intensive [9] [10] [11] [12]. For a given electric field E/N applied instantaneously to an electron swarm, the principal challenge is therefore to evaluate the electronic thermalisation time (τ_{th}). This key parameter can be then directly compared with the typical risetimes of fast voltage pulses with comparable peak electric fields. Such comparisons would allow the identification of operating criteria for the establishment of thermalised and non-thermalised plasmas under fast transient excitation, and thereby provide a sound basis for selecting the appropriate numerical model based on either steady-state or time-dependent Boltzmann codes. In addition, knowledge of the EEDF relaxation time is also of topical importance for the experimental determination of the electric fields at sub-nanosecond resolution in fast transient plasmas [13] [14] [15] [16].

To date, studies of the temporal relaxation of the EEDF following the instantaneous application of an electric field with fixed amplitude have been reported only for a few select values of the electric field in a given gas, for example, E/N=60Td in He, Xe [12], E/N=1.5Td, 24Td and 60Td in Ne [11] [17], E/N=60Td in Ar [9], E/N=60Td in N_2 [12], E/N=76Td in N_2 [17], E/N=1000Td in N_2 [18], E/N=500Td in air [4], E/N=100Td, 300Td, 1000Td, and 3500Td in air [16]. Furthermore, τ_{th} values were evaluated in only a few cases [12] [17] [18], but in one instance were also found to have a significant dependence on E/N [16]. To undertake a more comprehensive study, we have calculated the time taken for electrons to become thermalised for a given E/N over a broad range of fields 1Td<E/N<1000Td which are applicable to most weakly-ionised medium- to high-pressure plasma discharges. We have numerically solved the multi-term, spatially-homogenous Boltzmann equation [19], subject to an instantaneously applied but thereafter constant (time-independent) electric field, to follow the EEDF as it evolves from an initial room-temperature Maxwellian distribution toward the steady-state. Transport quantities such as the mean electron energy $\langle\varepsilon\rangle$ and electron drift velocity W_e have been calculated at each time, together with the volume production rates for electronic excitation k_{ex} and ionisation k_i. These swarm parameters are tracked in time until they converge to steady-state values. Finally, an overall thermalisation time is defined in terms of the time taken for the slowest evolving parameter to reach a satisfactory level of convergence. Xenon was chosen as the target gas for two reasons; firstly, fast-risetime pulsed medium-pressure Xe plasmas have been investigated extensively for use as efficient vacuum-ultraviolet (λ~172nm) lamps [20] [21] [22], and secondly, understanding the time-evolution of the EEDF toward thermalisation in the presence of large variations in the electron momentum transfer cross-section associated with the deep Ramsauer minimum in a heavy rare-gas [23] is of particular interest [24]. Lastly, fast transient plasmas operating with peak voltages substantially higher than the minimum breakdown voltage may utilise very high electric fields E/N=10^3-10^4Td [25], and an additional manifestation of non-equilibrium type behaviour will be associated with the production of high-energy runaway or ballistic electrons in the bulk plasma [18] [26]. However, the study of this regime is beyond the scope of the current work, and we have restricted the present calculations to electric fields below E/N<1000Td. Previous Monte-Carlo studies [27] [28] suggest no significant production of runaway electrons occurs for electric fields below this limit.

We begin this paper by describing the time-dependent Boltzmann code in section 2. A discussion of the convergence of the EEDF and transport properties with the number of Legendre polynomial terms is given in section 3.1. The results showing the time-evolution and ultimate convergence of the EEDFs and swarm parameters towards steady-state in response to an applied electric field (heating phase) are given in section 3.2. A brief analysis of the thermalisation of the EEDF following the removal of an electric field (the cooling phase) is given in section 3.3. A comparison between our evaluated τ_{th} values and the nanosecond pulse risetimes used in several experimental systems in given in section 3.4. Finally, the results are summarised in section 4.

2. Multi-term solution of Boltzmann's equation

2.1 Theory

The fundamental kinetic equation used in this paper (and previously [29] [30] [31]) for describing the electron swarm

evolution is the spatially-homogenous Boltzmann equation for the velocity-space distribution function, $f \equiv f(\boldsymbol{v}, t)$ [32] i.e.,

$$\left(\frac{\partial}{\partial t} + \frac{e\boldsymbol{E}}{m_e} \cdot \frac{\partial}{\partial \boldsymbol{v}}\right) f = -J(f), \tag{1}$$

where t is the time, $\boldsymbol{v}$, e and m_e are the velocity, charge and mass of the electron respectively. $J(f)$ represents the Boltzmann collision operator, and describes the effect of collisions on the distribution function [33]. Solving equation (1) for the distribution function yields the relevant information about the system, e.g. macroscopic transport properties such as mean energy, drift velocity and average collision rates can then be found via averages over the ensemble as detailed in equations (6)-(9).

The application of an electric field introduces a preferred direction into the electron system, such that the angular dependence of the velocity component can be represented by a Legendre polynomial expansion [34], i.e. $f(\boldsymbol{v}, t) \equiv f(v, \mu, t)$ where $\mu = \boldsymbol{E} \cdot \boldsymbol{v}$, and

$$f(\boldsymbol{v}, t) = \sum_{l=0}^{\infty} f_l(v, t) P_l(\mu), \tag{2}$$

where P_l is the l-th Legendre polynomial [35]. Equation (1) can then be decomposed into the following set of coupled partial differential equations for the $f_l \equiv f_l(\varepsilon, t)$ in energy-space,

$$\frac{\partial f_l}{\partial t} + \sum_{p=\pm 1} \Delta_l^{(p)} \frac{eE}{m_e} \left(\varepsilon^{\frac{1}{2}} \frac{\partial}{\partial \varepsilon} + p \frac{\left(l + \frac{3p+1}{2}\right)}{2} \varepsilon^{-\frac{1}{2}} \right) f_{l+p} = -J_l(f_l) \tag{3}$$

where $\varepsilon = \frac{1}{2} m_e v^2$, J_l is the Legendre decomposition of the collision operator, and

$$\Delta_l^{(+1)} = \frac{(l+1)}{(2l+3)}, \tag{4a}$$

$$\Delta_l^{(-1)} = \frac{l}{(2l-1)}. \tag{4b}$$

In practice, one must truncate the series (2) at a sufficiently high index $l = l_{max}$. The history of charged particle transport in gases has been dominated by the "two-term approximation" [36], i.e., where only the first two terms have been included. The assumption of quasi-isotropy necessary for the two-term approximation is violated in many situations, particularly when inelastic collisions are included [37] or when higher order moments are probed [29]. Such an assumption is not necessary in our formalism. Rather, l_{max} is treated as a free parameter to be increased until some convergence or accuracy criterion is met. Further discussion on the l_{max} requirements for electrons in Xe is given in section 3.1.

To solve equation (3) we require the collision operators for all of the relevant collision processes, and their representations in terms of Legendre polynomials, J_l. In this work we assume a weakly-ionised plasma, akin to pre-breakdown conditions, and consider elastic, electronic excitation and ionisation collisions. e-e Coulomb collisions, and e-Xe* de-excitation collisions, are not included. If we assume that the neutral background gas is at rest and in thermal equilibrium at a temperature T_g, then the background medium has a Maxwellian distribution in velocity-space such that the collision operator is linear [33] i.e.,

$$J = J^{el} + J^{ex} + J^{i}. \tag{5}$$

The explicit form of the various collision operator components are given in the Appendix.

The collision operators incorporate microscopic scattering information via scattering cross-sections. The set of electron

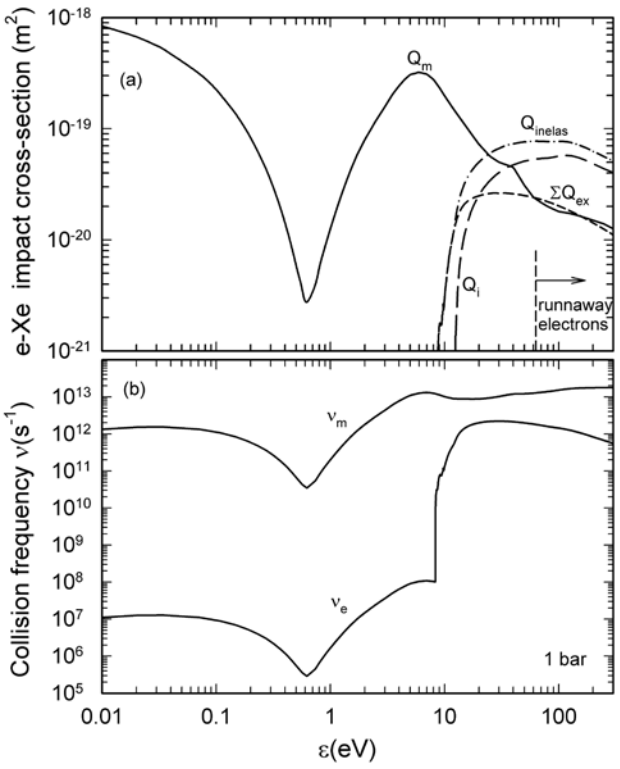

Figure 1. (a) Electron impact cross-sections for xenon from [38] as a function of electron energy ε: elastic momentum transfer - $Q_m(\varepsilon)$, total excitation summed over all Xe* excited states - $\Sigma Q_{ex}(\varepsilon)$, ionisation to Xe^+ - $Q_i(\varepsilon)$, and total inelastic - $Q_{inelas}(\varepsilon) = \Sigma Q_{ex}(\varepsilon) + Q_i(\varepsilon)$. Runaway electrons can occur for energies where $Q_{inelas}(\varepsilon)$ falls with increasing ε (i.e. ε>63eV in Xe). (b) Electron collision frequencies for elastic momentum transfer - $\nu_m(\varepsilon)$, and energy dissipation - $\nu_e(\varepsilon)$ at atmospheric pressure.

impact cross-sections for xenon were taken from the LXCat database [38], and are shown collectively in figure 1(a). Note that each inelastic cross-section is treated separately in the Boltzmann calculations. The associated collision frequencies for momentum transfer $\nu_m(\varepsilon)$ and for energy dissipation $\nu_e(\varepsilon)$ have been calculated using the formulae in [17], and are given in figure 1(b).

A ballpark estimate of the thermalisation time of the electrons in a *cooling* plasma (field-free) can be easily calculated from the inverse of the collision frequency for energy dissipation $\tau_{th}\sim 1/\nu_e$ [17] [39]. Such estimates have also been directly compared with the risetimes of pulsed electric fields [1] [15] [16] in order to gauge whether the electrons are thermalised in the *heating* phase of fast transient plasmas. However, it is not clear whether the kinetic processes associated with electron thermalisation are necessarily the same for both the cooling and heating phases. In fact, the results in [17] for Ne and N_2 (at E/N~30Td and E/N=76Td, respectively) suggest that τ_{th} values can be 1-2 orders of magnitude larger for the cooling phase than for the heating phase. We will examine this issue briefly for the case of xenon in section 3.3.

The macroscopic quantities of interest in this work are the electron number density n_e, flux drift velocity W_e, mean energy $\langle\varepsilon\rangle$, and the excitation k_{ex} and ionisation k_i coefficients, which can be calculated from the EEDF via [33],

$$n_e(t) = 2\pi\left(\frac{2}{m_e}\right)^{\frac{3}{2}}\int_0^\infty \varepsilon^{\frac{1}{2}} f_0(\varepsilon,t)\,d\varepsilon, \tag{6}$$

$$W_e(t) = \frac{1}{n_e}\frac{2\pi}{3}\left(\frac{2}{m_e}\right)^{2}\int_0^\infty \varepsilon f_1(\varepsilon,t)\,d\varepsilon, \tag{7}$$

$$\langle\varepsilon\rangle(t) = \frac{1}{n_e}2\pi\left(\frac{2}{m_e}\right)^{\frac{3}{2}}\int_0^\infty \varepsilon^{\frac{3}{2}} f_0(\varepsilon,t)\,d\varepsilon, \tag{8}$$

$$k_{ex}(t) = \frac{1}{n_e}2\pi\left(\frac{2}{m_e}\right)^{\frac{3}{2}}\int_0^\infty \Sigma\,\nu_{ex}(\varepsilon)\varepsilon^{\frac{1}{2}} f_0(\varepsilon,t)\,d\varepsilon \tag{9a}$$

and

$$k_i(t) = \frac{1}{n_e}2\pi\left(\frac{2}{m_e}\right)^{\frac{3}{2}}\int_0^\infty \nu_i(\varepsilon)\varepsilon^{\frac{1}{2}} f_0(\varepsilon,t)\,d\varepsilon, \tag{9b}$$

where ν_{ex} and ν_i are the collision frequencies for individual electronic excitations and for ionisation respectively, which are related to the corresponding cross-sections Q_{ex} and Q_i via

$$\nu_{ex,i}(\varepsilon) = NQ_{ex,i}(\varepsilon)\sqrt{\frac{2\varepsilon}{m_e}}. \tag{10}$$

The Σ in equation (9a) indicates the summation over all the electronic excitation processes.

A common theme in this work is the thermalisation (or relaxation) time. We define the parameter τ_{th} as the largest solution of

$$\left|1 - \frac{\varphi\left(\tau_{th}(X)\right)}{\varphi_{SS}}\right| = 1 - X, \tag{11}$$

where φ is one of the macroscopic transport quantities defined in equations (7)-(9), φ_{SS} is the associated steady-state value, and $X \in [0,1]$. τ_{th} for a given value of X then represents the time required for a transport coefficient φ to reach $(X \times 100)\%$ of the equilibrium value.

2.2 Numerical considerations and boundary conditions

The numerical techniques employed to solve the coupled system of partial differential equations (3) has been described previously [19] [29]. Briefly, equation (3) is discretised using a centred finite difference scheme in energy-space, and an implicit Euler scheme in time. We employ the boundary conditions recommended by the extensive studies of Winkler and co-workers [11] [40] [41] for the multi-term Legendre-decomposed Boltzmann equation, i.e.,

$$f_l(\varepsilon = 0, t) = 0, \quad \text{odd l} \tag{12a}$$
$$f_l(\varepsilon = \varepsilon_\infty, t) = 0, \quad \text{even l} \tag{12b}$$
$$f_l(\varepsilon > \varepsilon_\infty, t) = 0, \quad \text{all l} \tag{12c}$$

where ε_∞ represents a sufficiently large "cut-off" energy which is not known *a priori*. In practice we choose this cut-off value to be such that $f_0(\varepsilon_\infty, t) \le 10^{-10} \times \max\left(f_0(\varepsilon,t)\right)$, for all t.

The situation considered first is the "heating" of an ensemble of electrons in room-temperature (T_g=293K) thermal equilibrium with xenon gas via an instantaneously applied electric field. The initial EEDF is thus a thermal Maxwellian distribution f^{MW}:

$$f_0(\varepsilon, t=0) = f_0^{MW}(\varepsilon) \equiv \left(\frac{m_e}{2\pi k_b T_g}\right)^{\frac{3}{2}} e^{-\left(\frac{\varepsilon}{k_b T_g}\right)} \tag{13a}$$
$$f_l(\varepsilon, t=0) = 0 \quad l \ge 1 \tag{13b}$$

which has an initial average energy $\langle\varepsilon\rangle = \frac{3}{2}k_b T_g$, where k_b is the Boltzmann constant.

In section 3.3, the field-free "cooling" of the electron ensemble from the steady-state conditions achieved in the associated heating phase is considered. That is, the initial condition for $f_l(\varepsilon, 0)$ in the cooling phase is given by the numerical solution to the corresponding heating phase steady-state $f_l(\varepsilon, \infty)$.

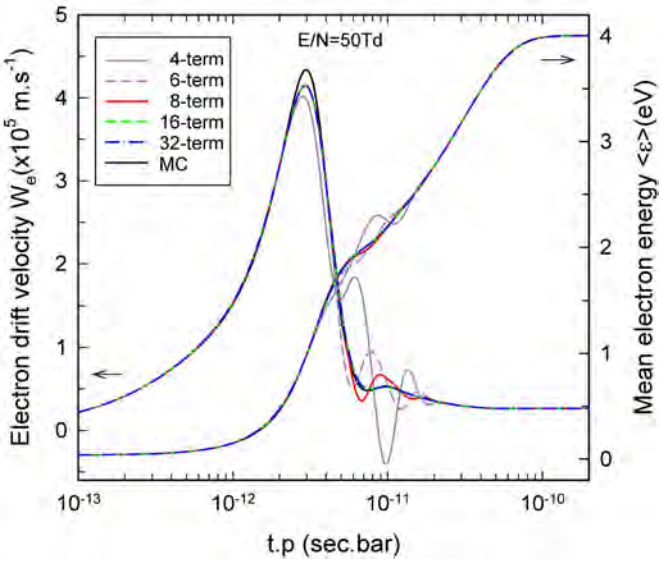

Figure 2. Temporal evolution of the electron drift velocity W_e and mean energy <ε> for a reduced field E/N=50Td using 4-, 6-, 8-, 16-, and 32-term approximations in the multi-term BE code, and the Monte-Carlo simulation.

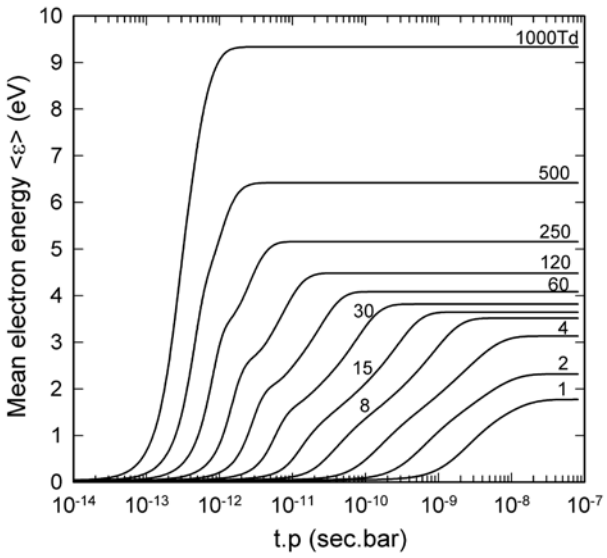

Figure 3. Time-evolution of the mean electron energy <ε> towards steady-state for selected values of the reduced electric field E/N.

3. Results and Discussion

3.1 Convergence: dependence on the number of Legendre terms

Initially, the time-dependent multi-term Boltzmann code was used to undertake a preliminary set of calculations for a typical field strength (E/N=50Td) to determine the influence (if any) of the number of terms of Legendre polynomials used to evaluate the swarm parameters. A set of results showing the evolution of the electron drift velocity W_e and the mean energy <ε> towards steady-state are shown in figure 2. For the 4-, 6- and 8-term approximations, both W_e and <ε> exhibit severe oscillatory behaviour around t.p~10^{-11}s.bar which is not seen when using the higher 16- and 32-term approximations. However, on reaching steady-state (t.p >10^{-10}s.bar), the values of W_e and <ε> are found to be identical for all five cases. The results for both the 16- and 32-term appear to be converged, and at all times differ by <1%. They are both in excellent agreement with the results from a Monte-Carlo simulation (see [42] for details). Overall, these findings are broadly consistent with the analogous multi-term BE calculations reported in [11] [12] for He and Ne at E/N=60Td. They evaluated EEDFs and swarm parameters using strict 2-, 4-, 6-, and 8-term approximations, and found that to achieve converged results over the full relaxation period required the use of 6-8 terms. They also reported [11] discrepancies indicating non-convergence of the EEDF in neon at higher fields E/N~150Td, despite using the 8-term approximation. In the current study, we have used the 16-term approximation to evaluate the set of swarm parameters for the range of reduced electric fields 1Td<E/N<1000Td (section 3.2). Despite the apparent convergence of the swarm parameter values at all times for our 16-term calculations, we did observe some residual discrepancies in the low energy region (ε<1.5eV) of the EEDF at E/N=50Td. These discrepancies were not observed when using the 32-term approximation, which was therefore adopted to evaluate the corresponding EEDFs. An apparent convergence of transport quantities despite failures in the distribution functions was previously demonstrated in [43] for ion transport.

For the cooling phase (section 3.3), the lack of electric field completely decouples the equations for the f_l components and we reverted to a 2-term approximation as the decoupled higher order terms do not contribute to the transport quantities considered in this paper.

3.2 Relaxation in a constant electric field (heating phase)

The time-dependence of the key swarm parameters <ε>, W_e, k_i, k_{ex} as they evolve towards their final steady-state values are shown collectively in figures 3-5 for selected values of the reduced electric field between 1-1000Td. It is immediately clear that the time signatures of the resulting curves are strongly dependent on the magnitude of the applied electric field, with the time to reach steady-state decreasing by around 5-orders of magnitude from ~10^{-7}s to 10^{-12}s (at 1bar Xe) as the field increases from E/N=1Td to 1000Td. By t.p~10^{-7}s.bar, the mean electron energies (figure 3) have reached their steady-state values for all chosen values of E/N,

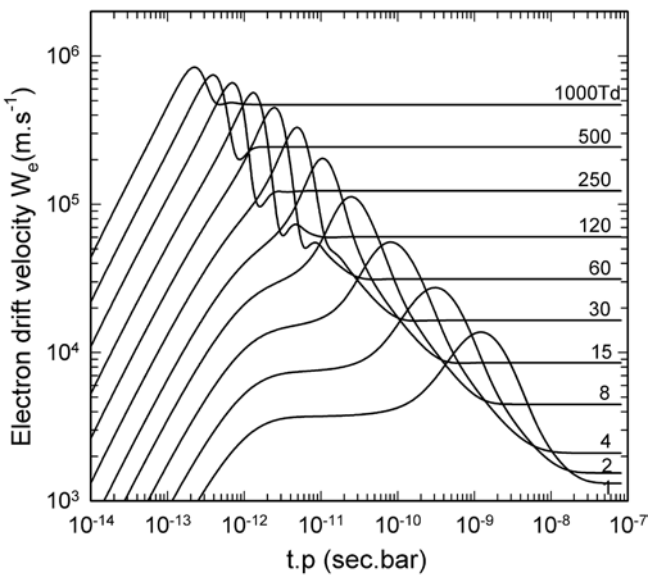

Figure 4. Time-evolution of the electron drift velocity W_e towards steady-state for selected values of the reduced electric field E/N.

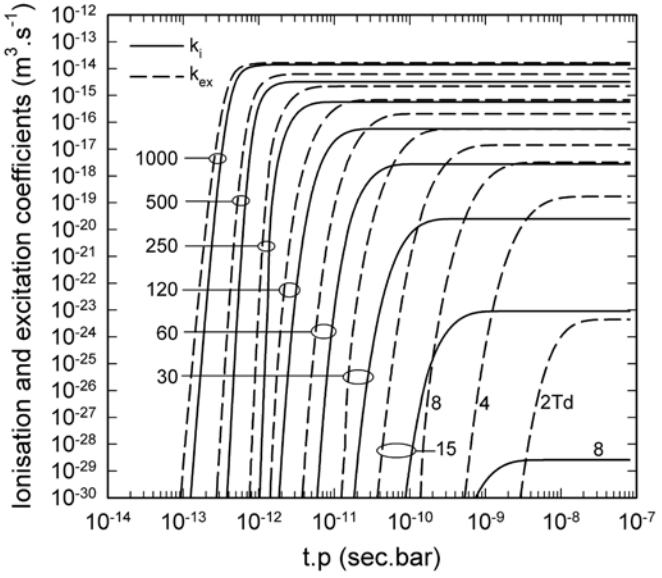

Figure 5. Time-evolution of the volumetric ionisation (k_i) and excitation (k_{ex}) coefficients towards steady-state for selected values of the reduced electric field E/N.

and they remain below 10eV, indicating that the majority of the electrons will have energies well below those normally associated with the runaway regime (figure 1(a)).

The time-dependences of the electron drift velocity W_e are shown in figure 4, and all generally follow the same behaviour although on differing time-scales. The drift velocities increase linearly initially, reach a peak value at an intermediate time, before falling back toward a constant steady-state value at later times. For low E/N≤4Td, W_e values also plateau for a brief period at early times. The overshoot in W_e is found to occur for all values of E/N, and can reach an order of magnitude or more above the final steady-state value when E/N<120Td. This tendency for the drift velocity to overshoot its steady-state value during relaxation has been reported previously in [9] for an applied field E/N=24Td, and in [44] for the case of a step-change in electric field (E/N=0.5Td to 1.0Td). It is discussed below in more detail for the case of a typical field E/N=50Td. The time-dependent behaviour of the ionisation and excitation coefficients are shown in figure 5 for the same range of E/N values. At low E/N (<60Td), the excitation coefficient is the dominant inelastic collision process (i.e. k_{ex}>>k_i), and it is consistently several orders of magnitude larger than the ionisation coefficient. The coefficients trend towards parity as the field increases up to E/N=1000Td. Overall, the results in figures 3-5 show that by t.p~10^{-7}s.bar, steady-state conditions are reached for the evolving swarm parameters for all values of E/N (>1Td). At steady-state, the corresponding set of field-dependent electron drift velocities $W_{e,ss}$ can be directly compared with experimental measurements, as shown in figure 6, as well as reduced Townsend coefficients α_T/N derived from the ionisation coefficients $k_{i,ss}$ and higher order terms as detailed in the caption. The current results are in excellent agreement with the measurements of W_e reported in [45] [46] [47] [48] covering 1Td<E/N<612Td. For the reduced Townsend ionisation coefficient, our results are in close agreement with those of [47] [49] [50] for 60Td<E/N<690Td, and in reasonable agreement (~25% higher) with the data in [51] for lower fields 25Td<E/N<36Td.

The electron thermalisation time τ_{th} can be evaluated by

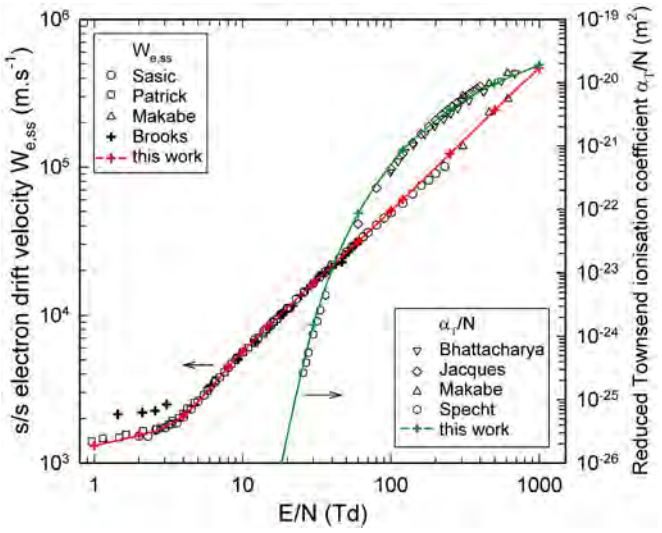

Figure 6. Steady-state (s/s) values of the electron drift velocity $W_{e,ss}$ and reduced Townsend ionisation coefficient α_T/N from the current work compared with experimental results of Sasic [45], Patrick [46], Makabe [47], Brooks [48], Bhattacharya [49], Jacques [50], and Specht (direct) [51] from the LAPLACE database [52]. The Townsend ionisation coefficient has been calculated to second order [53] from higher-order hydrodynamic quantities as described in [54] [55].

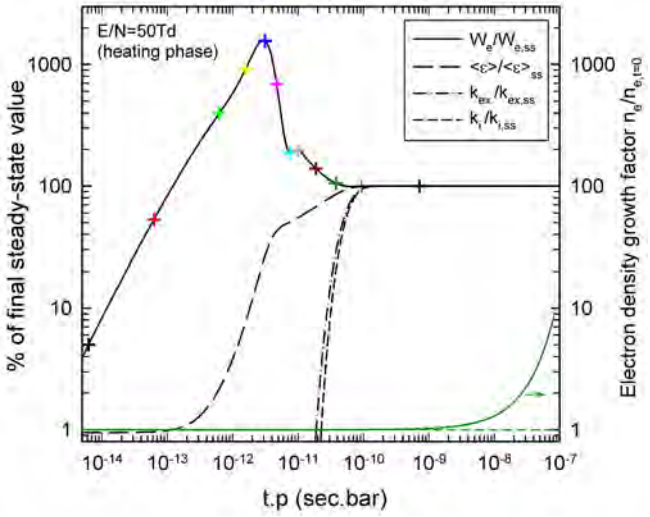

Figure 7. Time-evolution of the swarm parameters towards their final steady-state values for a reduced electric field E/N = 50Td. Indicative times are denoted by coloured crosses on the curve for $W_e/W_{e,ss}$, which correspond to EEDFs shown in figure 8. The cumulative growth of electron density $n_e/n_{e,t=0}$ is also shown (green line).

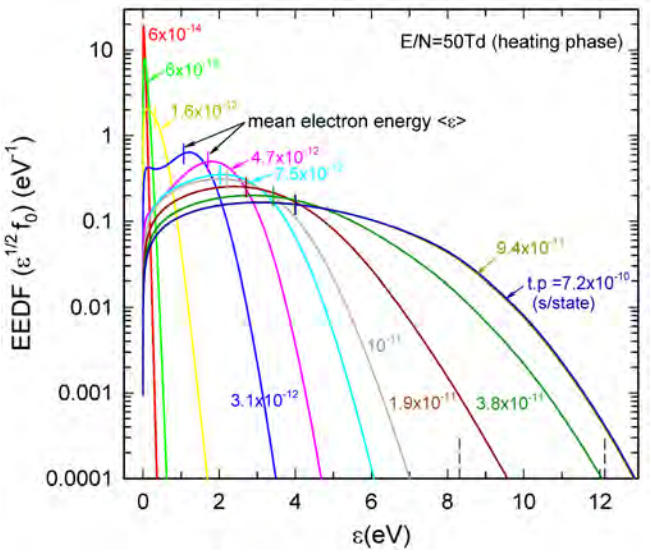

Figure 8. Electron energy distribution function (normalised) at E/N=50Td from 32-term calculations for selected times (in units sec.bar) towards steady-state, as also indicated in figure 7 (crosses). The energy thresholds for the lowest electronic excitation ($\Delta\varepsilon_{ex}$ =8.315eV) and for ionisation ($\Delta\varepsilon_i$=12.13eV) are shown as dashed lines.

first setting an appropriate benchmark to denote a satisfactory level of convergence of the swarm parameters towards their final steady-state values. However, it is also informative to understand the kinetic processes at play that lead to thermalisation. These two tasks can be undertaken by studying in detail the time-evolution of the various parameters for a typical (mid-range) value of the electric field, E/N=50Td.

3.2.1 Kinetic processes during thermalisation

A direct comparison of the degree of convergence of the swarm parameters towards steady-state values (at E/N=50Td) is shown in figure 7. The corresponding EEDF profiles at the selected times illustrated in figure 7 (crosses) are depicted in figure 8. Initially, W_e rises linearly with time and climbs to a transient peak at t.p~3x10^{-12}s.bar at which time the EEDF clearly contains a large fraction of electrons at energies ε=0.3-0.8eV, matching the Ramsauer minimum of $Q_m(\varepsilon)$ in Xe (figure 1(a)). It is well known that this cross-section minimum is directly linked to a significant (>20x) increase in electron mobility μ_e for weak DC fields E/N~0.03-1.0Td compared to the relatively constant value for higher fields E/N>4Td [46] [56]. For later times t.p>3x10^{-12}s.bar, electrons reach energies corresponding to the rapidly rising part of $Q_m(\varepsilon)$ (0.6<ε<6.0eV) resulting in a steady reduction of W_e (and μ_e) with time. At t.p~10^{-11}s.bar, W_e values exhibit a small plateau as electrons reach energies ε>6.0eV (corresponding to a decreasing $Q_m(\varepsilon)$ in figure 1(a)), before eventually falling toward their constant steady-state values at late times (t.p>10^{-10}s.bar). The EEDFs in figure 8 show that the low energy region ε=0-3eV converges toward steady-state well before the high energy region ε>8.3eV, the lowest threshold for inelastic collisions. This delay explains the relatively late rise of the ionisation k_i and excitation coefficients k_{ex} in figure 7 (i.e. t.p>2x10^{-11}s.bar). We also note that despite the ionisation coefficient reaching its steady-state value by t.p~10^{-10}s.bar, electron multiplication/growth does not begin significantly until considerably later at t.p~10^{-9}s.bar, i.e. the timescale set by ionisation is much larger than the time to reach the steady-state ionisation rate.

Lastly, we make two minor observations. Firstly, for the steady-state EEDF (t.p=7.2x10^{-10}s.bar), the fraction of high energy electrons at ε>63eV (figure 1(a)) is entirely negligible. Even at the highest field E/N=1000Td, this fraction rises to ~0.04%, thus we find no evidence of runaway electrons for fields up to 1000Td, confirming the results in [27]. Secondly, we do not see any evidence of a reversal of polarity of the drift velocity at early times, as found in the numerical simulations in [12] (for Xe at E/N=60Td) and [9] (for Ar at E/N=60Td) in the case of an instantaneously applied electric field. However, our finding is also consistent with previous reports [9] [57] that associate the appearance of a transient negative drift velocity with the adoption of a starting EEDF (at t=0) containing only relatively high energy electrons (e.g. ε=14-16eV [12]; ε=4.5-6.5eV [9]). Under such conditions, the EEDF acquires an "inverse shape" with $df_0/d\varepsilon>0$ at electron energies slightly higher than the Ramsauer minimum, as discussed by [24]. Our initial EEDF has comparatively low mean energy <ε>~0.038eV.

Steady-state conditions are ultimately reached at late times when the energy gain and loss processes for the electron

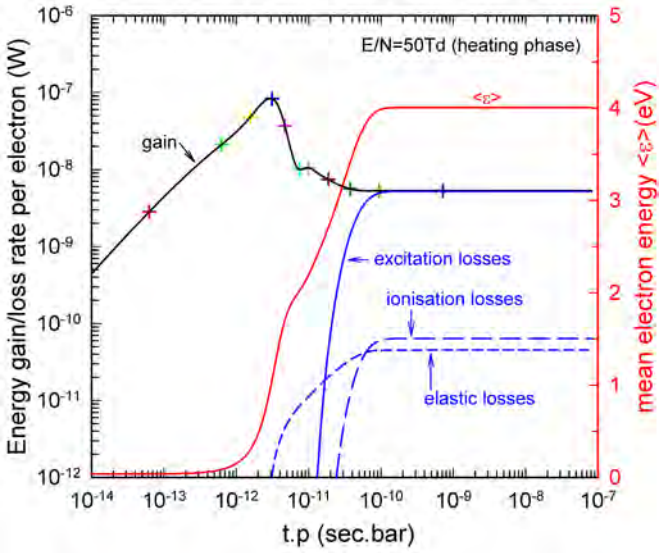

Figure 9. Energy gain (W_e.e.E), excitation losses $\Sigma(<Q_{ex}.v>.N.\Delta\varepsilon_{ex})$ ionisation losses $<Q_i.v>.N.\Delta\varepsilon_i$ ($\Delta\varepsilon_i$=12.13eV+<ε>), and "elastic losses" $2m_e/M <\nu_m(\varepsilon - 1.5k_bT_g)>$.

swarm come into balance, as depicted in figure 9 for E/N=50Td in the region t.p>10^{-10}s.bar. Of the energy gained by the electrons from the electric field, it is clear that it is mostly lost through excitation process to produce Xe* states (~98%), with ionisation and elastic collisions each accounting for ~1%. Moreover, across the range of reduced electric fields 1-1000Td under current investigation, the principal energy losses at steady-state are collectively through inelastic collisions, as shown in table 1. Elastic collisions are only important for fields E≤25Td, but become the dominant loss mechanism for E/N<6Td. Thus, a key result from this study is that for applied electric fields 25Td<E/N<1000Td, steady-state conditions are reached during the process of thermalisation when energy gained from the electric field is almost entirely balanced by energy losses due to *inelastic* collisions.

E/N (Td)	Ionisation (%)	Excitation (%)	Inelastic (% total)	Elastic (%)
1000	64.9	35.1	100.0	<0.01
250	31.9	68.1	100.0	<0.05
50	1.2	97.9	99.1	0.9
25	<0.03	97.0	97.0	3.0
10	<0.01	83.5	83.5	16.5
8	0	74.7	74.7	25.3
6	0	56.0	56.0	44.0
5	0	39.2	39.2	60.8
4	0	17.1	17.1	82.9

Table 1. Fractional energy losses for an electron swarm in xenon at steady-state in reduced fields 4Td<E/N<1000Td.

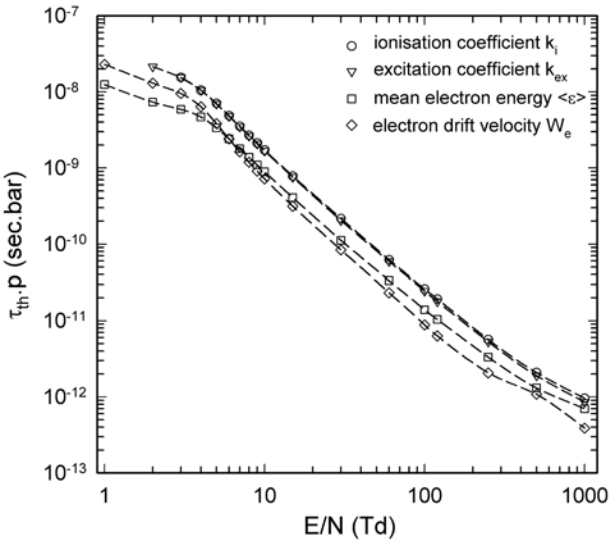

Figure 10. Thermalisation time (τ_{th}.p) as a function of the applied electric field E/N on the basis of the time taken for a given swarm parameter to reach 90% of its steady-state value. Note for E/N<3Td, the value of k_i is undefined. For E/N=1Td, the value of k_{ex} is undefined.

3.2.2 Criterion for evaluating thermalisation time τ_{th}

For a typical electric field of E/N=50Td, the results in figure 7 indicate that the drift velocity W_e is the first parameter to reach a steady-state, closely followed by the mean energy <ε>, and then in order the excitation and ionisation coefficients k_{ex} and k_i. The slight differences in convergence times have a significant impact. For example at $4.6x10^{-11}$s.bar, the convergence of $W_e/W_{e,ss}$ and $<\varepsilon>/<\varepsilon>_{e,ss}$ both exceed 90%, but $k_{ex}/k_{ex,ss}$ and $k_i/k_{i,ss}$ are only partially converged, at 45% and 27%, respectively.

The thermalisation time for an individual swarm parameter to reach 90% of its final value at steady-state is shown in figure 10 for 1Td<E/N<1000Td. For E/N<3Td, the value of k_i is undefined as the magnitude of the EEDF sampling the ionisation cross-sections is below the cut-off threshold. For E/N=1Td, both k_i and k_{ex} are undefined. For a given E/N, the results show that the four parameters have a spread of individual thermalisation times that are consistently within a factor of ~2.5x when comparing the fastest and the slowest to converge. An acceptable measure of the relaxation of the electron swarm requires that the overall thermalisation time be chosen on the basis of the parameter φ that is last to converge. Thus, we use the ionisation coefficient $\varphi=k_i$ for 3Td<E/N<1000Td, the excitation coefficient $\varphi=k_{ex}$ for E/N=2Td, and the drift velocity $\varphi=W_e$ for E/N=1Td. The calculated thermalisation time τ_{th}.p representing the convergence of φ toward its final value at steady-state is shown in figure 11 for fields 1Td<E/N<1000Td, and for

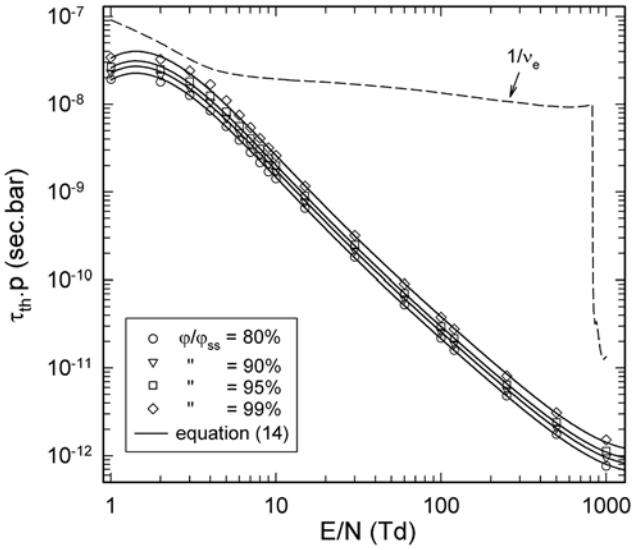

Figure 11. Thermalisation time (τ_{th}.p) as a function of the applied electric field E/N on the basis of the time taken for the slowest converging parameter φ to reach a given percentage of its steady-state value φ_{SS}. Solid lines are calculated from equation (14). The inverse of the collision frequency for energy dissipation ($1/\nu_e(\langle\varepsilon\rangle)$) at p=1bar is also shown (dashed line).

various degrees of convergence of 80%, 90%, 95% and 99%. The resulting values of τ_{th}.p in figure 11 are found to vary by almost 5 orders of magnitude over the 3 order-of-magnitude range of the reduced electric field. Nevertheless, the data points can be closely fitted by the following formula, which additionally allows τ_{th}.p to be evaluated according to the desired level of convergence of φ/φ_{SS} between 80% and 99%:

$$\tau_{th}.p\ (sec.bar) = 2.2608\times10^{-8}\left[ln\left(\beta\left(\frac{X}{1-X}\right)^{\gamma}\right)\right] \times exp\left[\sum_{n=1}^{n=5}\phi_n\left(ln\left(\frac{E}{N}\right)\right)^n\right] \quad (14)$$

where X (with $0.8<X<0.99$) is the deviation of the value of φ from the asymptotic value at steady-state φ_{SS}, E/N is in Td, and β, γ and ϕ_n are dimensionless coefficients as follows: ϕ_1=1.0706, ϕ_2=-1.7721, ϕ_3=0.48419, ϕ_4=-0.06156, ϕ_5=3.0306x10^{-3}, β=1.7424 and γ=0.20239.

Lastly, ballpark estimates of the thermalisation time evaluated from the inverse collision frequency for energy dissipation $1/\nu_e(\varepsilon)$ at 1bar (from figure 1(b)) are also shown in figure 11. We have taken ε as the mean energy of the EEDF at steady-state conditions (i.e. $\langle\varepsilon\rangle$=1.8-9.3eV). These ballpark estimates are clearly in poor agreement with our final results, except for low fields E/N<4Td. The cause of this disagreement can be understood from the results in section 3.2.1 which showed that for E/N>25Td, thermalisation times are predominantly linked to the rate of energy loss via inelastic collisions, thus involving only higher energy electrons with $\varepsilon>\Delta\varepsilon_{ex}$. This comparison suggests that thermalisation times for the heating phase derived directly from $1/\nu_e(\varepsilon)$ values, with ε chosen to represent a typical or average energy of the EEDF, are likely to be unreliable.

3.3 Field-free relaxation (cooling phase)

For comparison with the results in section 3.2.1 which described relaxation processes during the heating phase following the application of a typical electric field, we briefly analyse the analogous processes for a cooling plasma from the moment this electric field is instantaneously and completely removed (field-free). The scenario represents the idealised case of the evolution of a weakly-ionised plasma during the trailing edge of a nanosecond voltage pulse. In reality, if the magnitude of the applied electric field is sufficient to cause electrical breakdown, analysis of the subsequent relaxation of the plasma following the removal of the electric field should also include a number of secondary processes, notably e-e (Coulomb) collisions, de-excitation or superelastic collisions, recombination heating, and space-charge induced electric fields [20] [58]. However, the inclusion of these processes in BE calculations requires modelling of the temporal evolution of the species population densities (e.g. [n_e], [Xe^*], [Xe^{**}], [Xe^+]) which is beyond the scope of the current work. Previously, field-free relaxation of a weakly-ionised plasma following the instantaneous removal of an electric field has been investigated in [17] in Ne and N_2 whilst relaxation due to a step-reduction of an electric field has been studied in [59] for Ne and H_2. The influence of e-e Coulomb collisions on the relaxation of weakly ionised Xe plasmas (for field-free conditions) has been investigated in [24].

The temporal evolution of the swarm parameters immediately after removal of the electric field (50Td) is shown in figure 12. The corresponding EEDFs at selected times during the cooling phase are given in figure 13, whilst the associated energy loss processes are depicted in figure 14. At early times, it is clear that the drift velocity decays very quickly (figure 12), due to the large momentum transfer collision frequency, e.g. ν_m~10^{11}-$10^{13}$$s^{-1}$ at 1bar (figure 1(b)). High energy electrons ($\varepsilon>\Delta\varepsilon_{ex}$) dissipate their momentum the most rapidly (ν_m~$10^{13}$$s^{-1}$ at 1bar or τ~10^{-13}s.bar) whereas electrons with energy near the Ramsauer minimum (ε~0.6eV) lose their momentum more gradually (ν_m~$10^{11}$$s^{-1}$ at 1bar or τ ~10^{-11}s.bar). The fast decay of the drift velocity is immediately followed by the rapid depletion of high energy electrons in the EEDF ($\varepsilon>\Delta\varepsilon_{ex}$) due to inelastic collisions (figure 13), thereby effectively quenching the ionisation rate, and then the excitation rate (figures 12 and 14). This rapid quenching of the

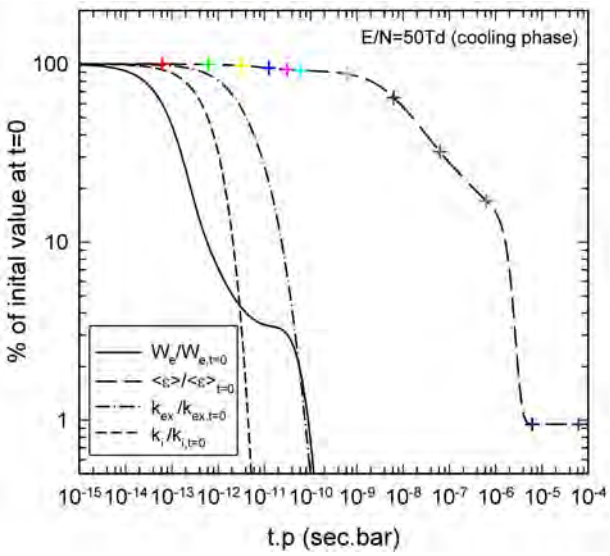

Figure 12. Time-evolution of the swarm parameters after removal of the electric field starting at steady-state values (at t=0) for E/N=50Td. Indicative times are denoted by crosses on the curve for $\langle\varepsilon\rangle/\langle\varepsilon\rangle_{t=0}$. Coloured crosses correspond to the EEDFs shown in figure 13.

high energy region of the EEDF is virtually complete by t.p=10^{-10}s.bar (consistent with the collision frequency for energy loss at 1bar $1/\nu_e \sim 10^{-10}$s at ε~8.5eV, figure 13). The plasma then begins a second (much slower) period of cooling as electrons with energies below the first excitation potential ($\varepsilon<\Delta\varepsilon_{ex}$) start to cool to ambient temperatures (ε~0.038eV). This second stage is characterised by a timescale 4-5

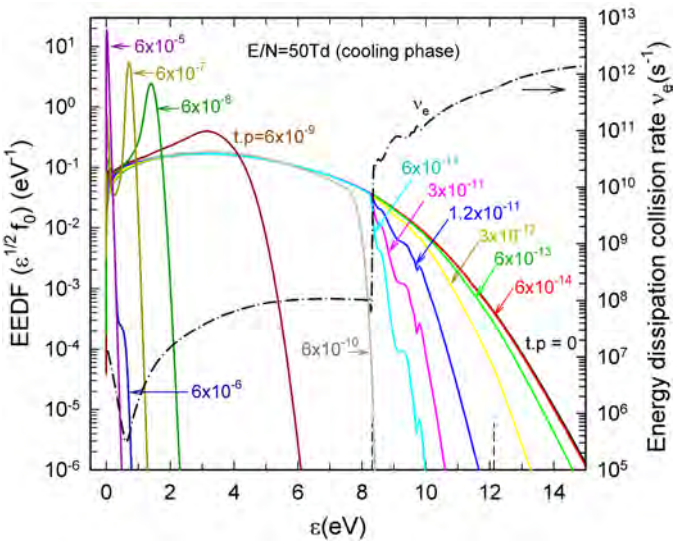

Figure 13. Electron energy distribution functions (normalised) at E/N=50Td for selected times (in units s.bar) after steady-state, as also indicated in figure 12 (crosses). The energy thresholds for the lowest electronic excitation ($\Delta\varepsilon_{ex}$=8.315eV) and for ionisation ($\Delta\varepsilon_i$=12.13eV) are shown as dashed lines, and the collision frequency for energy dissipation $\nu_e(\varepsilon)$ at p=1bar (chained line). Note: discontinuities in EEDFs between 8-10eV coincide with energy thresholds for different Xe* states.

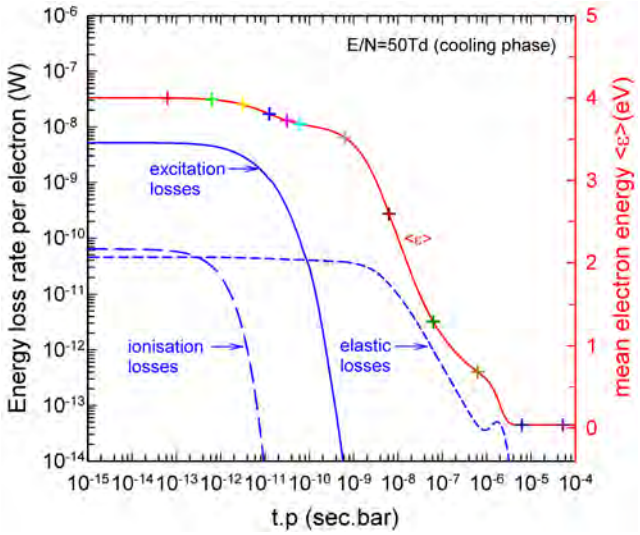

Figure.14. Excitation losses $\Sigma(\langle Q_{ex}.v\rangle.N.\Delta\varepsilon_{ex})$, ionisation losses $\langle Q_i.v\rangle N\Delta\varepsilon_i$ ($\Delta\varepsilon_i$=12.13eV+<ε>), and "elastic losses" $2m_e/M\ \langle\nu_m(\varepsilon - 1.5kT_g)\rangle$. Coloured crosses correspond to the EEDFs in figure 13.

magnitudes longer than that for both momentum dissipation and quenching of the inelastic collision rate, and the slow cooling rate is completely driven by the rate of the elastic collisions, as shown in figure 14. The slowed rate of cooling of <ε> between times t.p=10^{-7}-10^{-6}s.bar is due to electrons cooling to energies corresponding to the Ramsauer minimum, which effectively acts as bottleneck in terms of the overall relaxation time. A similar result for a cooling Xe plasma was reported in the numerical modelling in [24]. They also found that the bottleneck could be partially alleviated by including e-e collisions into their model with a fractional ionisation [e]/[Xe]=10^{-7}.

Lastly, applying the criterion that the thermalisation time be derived from the slowest evolving swarm parameter, τ_{th} for the cooling phase of the plasma must be defined in terms of the decay of the mean energy <ε> (figure 12) instead of k_i as used for the heating phase. In the case of E/N= 50Td, the time taken for <ε> to fall by 90% towards the thermal equilibrium value in a cooling plasma yields τ_{th}.p =1.632x10^{-6}s.bar. This is very close to a ballpark value estimated from the reciprocal of the slowest energy dissipation rate $(1/\nu_e)\sim 3.2\text{x}10^{-6}$ at 1bar and ε~0.6eV (figure 13). However, compared to our calculated thermalisation time for the heating phase at E/N=50Td τ_{th}.p=8.53x10^{-11}s.bar (figure 11), the relaxation time for the cooling phase is around ~20,000 times slower.

3.4 Comparison of thermalisation times with "nanosecond" excited plasmas (experimental)

In table 2, we summarise the operating conditions for several experimental fast-pulse excited plasma discharge systems. These medium- to high-pressure Xe_2^* excimer lamps are based on micro hollow-cathode or dielectric barrier

Ref.	Pressure p(bar)	E/N (Td) at voltage peak	Voltage pulse risetime τ_{rise}(ns)	τ_{th}(ns)	τ_{rise}/τ_{th}
Moselhy [60]	0.53	150-275	4	0.025-0.0094	160-425
Moselhy [21]	0.53	570	10	0.0032	3100
Lee [61]	0.8	300	6	0.0054	1100
Carman [62]	0.5-2.5	140-65	100	0.03-0.022	3300-4500

Table 2. Comparison of the risetimes of "nanosecond" voltage pulses in xenon from experiment (τ_{rise}) and calculated electron thermalisation times τ_{th} from equation (14) for X=90%, at the same E/N and gas pressure.

discharges, and are used to generate vacuum-ultraviolet light at λ~172nm [21] [60] [61] [62]. The discharges all utilise fast-pulse voltage waveforms evolving at nanosecond timescales to achieve optimal performance in terms of VUV output and electrical efficiency. Fundamentally, if the risetime (τ_{rise}) of the high-voltage pulse applied to the discharge is demonstrably slower than the calculated thermalisation time (τ_{th}) for the heating phase, then the EEDF will be fully thermalised during the entire leading edge of voltage pulse. The results in table 2 clearly show that for these experiments, $\tau_{rise}>>\tau_{th}$ (or $\tau_{rise}/\tau_{th}>>1$), so in all cases the EEDF would have been fully thermalised. Furthermore, since all τ_{th} values are found to fall in the range 3-30ps, a further reduction of the experimental risetimes to τ_{rise} to ~1ns (i.e. through the use of faster pulse generators [63]) would not, in these cases, lead to non-thermalised plasmas.

4. Conclusion

We have evaluated the thermalisation time for an electron swarm in gaseous Xe using a multi-term time-dependent Boltzmann equation, for a range of instantaneously applied reduced electric fields 1Td<E/N<1000Td. Starting from a Maxwellian shaped EEDF at room temperature at a given E/N, the time-evolution of the distribution function and associated electron swarm parameters (drift velocity W_e, mean energy $<\varepsilon>$, ionisation coefficient k_i, and excitation coefficient k_{ex}) were followed as they converged to steady-state values. Initially, we trialled 4-, 6-, 8-, 16-term, and 32-term BE calculations together with a Monte-Carlo simulation. The 4-, 6-, and 8-term calculations gave rise to oscillatory behaviour in W_e and $<\varepsilon>$ at intermediate times, which was mitigated using a higher number of terms or the MC method. Thus, the main results in this study were evaluated using 16-term and 32-term BE calculations. Steady-state values for both W_e and the reduced Townsend ionisation coefficient (α_T/N) have been verified against recent experimental measurements and were found to be in excellent agreement. For the range of electric fields 25Td<E/N<1000Td, the thermalisation process (during the heating phase) was completed when energy supplied to the electrons from the electric field came into balance with the energy losses predominantly due to inelastic collisions. For very low fields E/N<6Td, energy gained by electrons from the electric field was balanced by energy losses mainly due to elastic collisions. For all values of E/N, the individual swarm parameters were found to converge towards their steady-state values at slightly different rates. For E/N>5Td they converge in order W_e (fastest), $<\varepsilon>$, k_{ex}, and k_i (slowest). The time taken for the slowest swarm parameter to converge to an acceptable level (e.g. to within 90% of its steady-state value) was used universally as the benchmark for evaluating the thermalisation time τ_{th}. This time was found to be strongly dependent on the value of the reduced electric field E/N, dropping by almost 5 orders of magnitude for increasing electric fields 1Td<E/N<1000Td. As a key outcome from this work, the calculated thermalisation times τ_{th}.p (s.bar) have been expressed as a general formula, as a function of both the reduced electric field E/N and a user defined convergence level between 80-99%. We have also shown that ballpark estimates of thermalisation times, based on the inverse of the collision frequency for energy dissipation ($1/\nu_e(\varepsilon)$) at typical average electron energies, are likely to be unreliable if applied to the heating phase.

We also undertook a brief analysis of the cooling phase when the electric field was instantaneously removed from the plasma (i.e. field-free) after it had evolved to steady-state conditions during the previous heating phase. For a typical electric field E/N=50Td, the EEDF was found to relax in two distinct stages. Initially, the high energy region of the EEDF above the lowest excitation energy $\varepsilon>\Delta\varepsilon_{ex}$ was rapidly depleted due to inelastic collisions. The lower part of EEDF $\varepsilon<\Delta\varepsilon_{ex}$ cooled over a substantially longer time period (several orders of magnitude slower than the first stage) being regulated by the energy losses associated with only elastic collisions. In this case, the last swarm parameter to reach a satisfactory convergence toward steady-state was the mean energy $<\varepsilon>$. The overall relaxation time of the plasma during the cooling period (field-free) was consistent with a ballpark estimate based on the inverse of the collision frequency for energy loss $\tau_{th}\sim1/\nu_e(\varepsilon)$ with ε~0.6eV (corresponding to the Ramsauer minimum in Xe).

Finally, we compared calculated thermalisation times with the typical risetimes of the voltage pulse waveforms for several experimental "nanosecond" pulse excited plasma discharge devices. The results showed in all cases that the EEDFs would have been fully thermalised during the leading edge of the voltage pulse. Further work to calculate the thermalisation times for the other rare gases Kr, Ar, Ne, He, as well as N_2 and O_2, is currently being undertaken for future publication.

Appendix

The solution to equation (3) requires explicit expressions for the Legendre-decomposition of the elastic, excitation and ionisation collision operator terms. The elastic collision operator, J_l^{el}, is given by the Davydov operator [64]:

$$J_l^{el}(f_l) = \begin{cases} -\dfrac{2m_e}{M}\varepsilon^{-\frac{1}{2}}\dfrac{\partial}{\partial\varepsilon}\left[\varepsilon^{\frac{3}{2}}\nu_{el}^1(\varepsilon)\left(f_0 + k_b T_g \dfrac{\partial f_0}{\partial\varepsilon}\right)\right] & l = 0 \\ \nu_{el}^l(\varepsilon) f_l(\varepsilon) & l \geq 1 \end{cases} \quad (A1)$$

where M is the mass of the neutral background particles, and

$$\nu_{el}^l(\varepsilon) = N\sqrt{\frac{2\varepsilon}{m_e}}\left(2\pi\int_{-1}^{1} Q(\varepsilon,\mu)[1 - P_l(\mu)]\, d\mu\right), \quad (A2)$$

where $Q(\varepsilon,\mu)$ is the differential elastic scattering cross section. $\nu_{el}^1 \equiv \nu_m$ can be identified as the well-known momentum-transfer collision frequency.

The collision operator for a given conservative inelastic process, which in this work only encompasses electronic excitations, J_l^{ex}, is given by the Wang-Chang *et-al* semiclassical operator [65]:

$$J_l^{ex}(f_l) = \begin{cases} \nu_{ex}(\varepsilon) f_0(\varepsilon) - \left(\dfrac{\varepsilon'}{\varepsilon}\right)^{\frac{1}{2}} \nu_{ex}(\varepsilon') f_0(\varepsilon') & l = 0 \\ \nu_{ex}(\varepsilon) f_l(\varepsilon) & l \geq 1 \end{cases} \quad (A3)$$

where $\varepsilon' = \varepsilon + \Delta\varepsilon_{ex}$, $\Delta\varepsilon_{ex}$ is the threshold energy for the excitation and ν_{ex} is given in equation (10). Here super-elastic collisions have been neglected by virtue of the threshold energy being large compared to the background gas thermal energy.

In contrast to elastic and excitation collisions, electron-impact ionisation is a particle non-conserving process. For the simplest case of the post-ionisation energy being shared equally between the (indistinguishable) scattered and ejected electrons the ionisation collision operator is [66]:

$$J_l^{i}(f_l) = \begin{cases} \nu_i(\varepsilon) f_0(\varepsilon) - \left(\dfrac{\varepsilon''}{\varepsilon}\right)^{\frac{1}{2}} \nu_i(\varepsilon'') f_0(\varepsilon'') & l = 0 \\ \nu_i(\varepsilon) f_l(\varepsilon) & l \geq 1 \end{cases} \quad (A4)$$

where $\varepsilon'' = \frac{\varepsilon}{2} + \Delta\varepsilon_i$, $\Delta\varepsilon_i$ is the threshold energy for the excitation and ν_i is given in (10). Electron-impact ionisation is not especially sensitive to the exact form of the post-ionisation energy-sharing [29] [67].

References

[1] S. Nagaraja, V. Yang and I. Adamovich, "Multi-scale modelling of pulsed nanosecond dielectric barrier plasma discharges in plane-to-plane geometry," *J.Phys.D: Appl. Phys.*, vol. 46, p. 155205, 2013.

[2] G. J. M. Hagelaar and L. C. Pitchford, "Solving the Boltzmann equation to obtain electron transport coefficients and rate coefficients for fluid models," *Plasma Sources Sci. Technol.*, vol. 14, pp. 722-733, 2005.

[3] M. Capitelli, C. Gorse, J. Wilhelm and R. Winkler, "Collision doiminated relaxation of electrons in a weakly ionised nitrogen plasma after abrupt change the electric field," *Chemical Physics*, vol. 79, pp. 1-7, 1983.

[4] M. Uddi, N. Jiang, E. Mintusov, I. V. Adamovich and W. R. Lempert, "Atomic oxygen measurements in airand air/fuel nanosecond pulse discharges by two photon laser induced fluorescence," *Proc. Combust. Inst*, vol. 32, pp. 929-36, 2009.

[5] R. Morrow, "Theory of negative corona in oxygen," *Physical Review A*, vol. 32, no. 3, p. 1799, 1985.

[6] T. B. Petrova, G. M. Petrov, D. R. Boris and S. G. Walton, "Non-equilibrium steady-state kinetics of He-air atmospheric pressure plasmas," *Physics of Plasmas*, vol. 24, p. 013501, 2017.

[7] J. Poggie, I. V. Adamovich, N. Bisek and M. Nishihara, "Numerical simulation of nanosecond-pulse electrical discharges," *Plasma Sources Sci Technol.*, vol. 22, p. 015001, 2013.

[8] R. Brandenburg, P. J. Bruggeman and S. M. Starikovskaia, "Fast Pulse Discharges (Special Issue: 20 papers)," *Plasma Sources Sci. Technol.*, vol. 26, p. 020201, 2017.

[9] D. Trunec, Z. Bonaventura and D. Necas, "Solution of time-dependent Boltzmann equation for electrons in non-thermal plasma," *J.Phys.D: Appl. Phys*, vol. 39, pp. 2544-2552, 2006.

[10] D. Loffhagen and R. Winkler, "A New Nonstationary Boltzmann Solver in Self-Consistent Modelling of Discharge Pumped Plasmas for Excimer Lasers," *J. Computational Phys.*, vol. 112, pp. 91-101, 1994.

[11] D. Loffhagen and R. Winkler, "Time-dependent multi-term approximation of the velocity distribution in the temporal relaxation of plasma electrons," *J.Phys.D: Appl. Phys*, vol. 29, pp. 618-627, 1996.

[12] D. Loffhagen and R. Winkler, "Multi-term treatment of the temporal electron relaxation in He, Xe and plasmas," *Plasma Sources Sci. Technol.*, vol. 5, p. 710, 1996.

[13] M. S. Simeni, B. M. Goldberg, C. Zhang, K. Frederickson, W. R. Lempert and I. V. Adamovich, "Electric field measurements in a nanosecond pulse discharge in atmospheric air," *J. Phys.D: Appl. Phys*, vol. 50, p. 184002, 2017.

[14] M. S. Simeni, B. M. Goldberg, I. Gulko, K. Frederickson, W. R. Lempert and I. V. Adamovich, "Sub-nanosecond resolution electric field measurements during ns pulse breakdown in ambient air," *J.Phys.D: Appl. Phys.*, vol. 50, p. 01LT01, 2018.

[15] T. Hoder, M. Cernak, J. Paillol, D. Loffhagen and R. Brandenburg, "High-resolution measurements of the electric field at the streamer arrival to the cathode: A unification of the streamer-initiated gas-breakdown mechanism," *Physical Review E*, vol. 86, p. 055401(R), 2012.

[16] T. Hoder, D. Loffhagen, J. Vorac, M. M. Becker and R. Brandenburg, "Analysis of the electric field development and the relaxation of electron velocity distribution function for nanosecond breakdown in air," *Plasma Sources Sci. Technol.*, vol. 25, p. 025017, 2016.

[17] R. Winkler, D. Loffhagen and F. Sigeneger, "Temporal and spatial relaxation of electrons in low temperature plasmas," *Applied Surface Sci.*, vol. 192, pp. 50-71, 2002.

[18] Y. M. Li, "Non-equilibrium effects in electron transport at high E/N," in *Non-equilibrium effects in electron and ion transport*, New York, Plenum Press, 1990, pp. 99-120.

[19] G. J. Boyle, W. J. Tattersall, D. G. Cocks, R. P. McEachran and R. D. White, "A multi-term solution of the space–time Boltzmann equation for electrons in gases and liquids," *Plasma Sources Sci. Technol.*, vol. 26, p. 024007, 2017.

[20] R. J. Carman and R. P. Mildren, "Computer modelling of a short-pulse excited dielectric barrier discharge xenon excimer lamp ($\lambda \sim 172$ nm)," *J.Phys.D: Appl. Phys.*, vol. 36, pp. 19-33, 2003.

[21] M. Moselhy, W. Shi, R. H. Stark and K. H. Schoenbach, "Xenon excimer emission from pulsed microhollow cathode discharges," *Applied Physics Lett.*, vol. 79, p. 1240, 2001.

[22] S. Beleznai, I. Mihajlik, I. Maros, L. Bal'azs and P. Richter, "Improving the efficiency of a fluorescent Xe dielectric barrier light source using short pulse excitation," *J.Phys.D: Appl.Phys.*, vol. 41, p. 115202, 2008.

[23] M. Suzuki, T. Taniguchi, N. Yoshimura and H. Tagashira, "Momentum transfer cross section of xenon deduced from electron drift velocity data," *J.Phys.D: Appl.Phys.*, vol. 25, pp. 50-56, 1992.

[24] Z. Donko and N. Dyatko, "First-principles particle simulation and Boltzmann equation analysis of negative differential conductivity and transient negative mobility effects in xenon," *European Phys. J. D*, vol. 70, p. 135, 2016.

[25] P. Tardiveau, L. Magne, E. Marode, K. Ouaras, P. Jeanney and B. Bournonville, "Sub-nanosecond time resolved light emission study for diffuse discharges in air under steep high voltage pulses," *Plasma Sources Sci. Technol.*, vol. 25, p. 054005, 2016.

[26] A. V. Phelps, B. M. Jelenkovic and L. C. Pitchford, "Simplified models of electron excitation and ionization at very high E/N," *Physical Review A*, vol. 36, no. 11, pp. 5327-5336, 1987.

[27] E. E. Kunhardt, Y. Tzeng and J. P. Boeuf, "Stochastic development of an electron avalanche," *Physical Review A*, vol. 34, no. 1, pp. 440-449, 1986.

[28] O. Chanrion and T. Neubert, "A PIC-MCC code for simulation of streamer propagation in air," *J. Computational Physics*, vol. 227, pp. 7222-7245, 2008.

[29] G. J. Boyle, W. J. Tattersall, D. G. Cocks, S. Dujko and R. D. White, "Kinetic theory of positron-impact ionization in gases," *Physical Review A*, vol. 91, p. 052710, 2015.

[30] G. J. Boyle, R. P. McEachran, D. G. Cocks and R. D. White, "Electron scattering and transport in liquid argon," *Journal of Chemical Physics*, vol. 142, p. 154507, 2015.

[31] G. J. Boyle, R. P. McEachran, D. G. Cocks, M. J. Brunger, S. J. Buckman, S. Dujko and R. D. White, "Ab initio electron scattering cross-sections and transport in liquid xenon," *J.Phys.D: Appl.Phys*, vol. 49, p. 355201, 2016.

[32] L. Boltzmann, "Lectures on Gas Theory," *Wien. Ber.*, vol. 66, p. 275, 1872.

[33] R. Robson, R. White and M. Hildebrandt, Fundamentals of Charged Particles in Gases and Condensed Matter, Boca Raton: CRC Press, 2017.

[34] R. E. Robson, R. Winkler and F. Sigeneger, "Multiterm spherical tensor representation of Boltzmann's equation for a nonhydrodynamic weakly ionized plasma," *Physical review E*, vol. 65, p. 056410, 2002.

[35] M. Abramowitz and I. A. Stegun, Handbook of Mathematical Functions, New York: Dover Publications Inc., 1972.

[36] L. G. H. Huxley and R. W. Crompton, The Drift and Diffusion of Electrons in Gases, New York: Wiley, 1974.

[37] R. D. White, K. F. Ness and R. E. Robson, "Development of swarm transport theory in radio-frequency electric and crossed electric and magnetic fields," *Applied Surface Sci.*, vol. 192, pp. 26-49, 2002.

[38] "LXCat, BIAGI database, Magboltz versions 8.9 and higher," [Online]. Available: http://www.lxcat.net. [Accessed 24 May 2018].

[39] S. O. Macheret, M. N. Shneider and R. B. Miles, "Modeling of Air Plasma Generation by Repetitive," *IEEE Trans. Plasma Sci.*, vol. 30, no. 3, pp. 1301-1314, 2002.

[40] R. Winkler, G. L. Braglia, A. Hess and J. Wilhelm, "Fundamentals of a Technique for Determining Electron Distribution Functions by Multi-Term Even-Order Expansion in Legendre Polynomials 1. Theory," *Beitr. Plasmaphys.*, vol. 24, pp. 657-674, 1984.

[41] H. Leyh, D. Loffhagen and R. Winkler, "A new multi-term solution technique for the electron Boltzmann equation of weakly ionized steady-state plasmas," *Computational Physics Commun.*, vol. 113, pp. 33-48, 1998.

[42] W. J. Tattersall, D. G. Cocks, G. J. Boyle, M. J. Brunger, S. J. Buckman, G. Garcia, Z. L. Petrovic, J. P. Sullivan and R. D. White, "Spatial profiles of positrons injected at low energies into water: influence of cross section models," *Plasma Sources Sci. Technol.*, vol. 20, p. 045010, 2017.

[43] D. A. Konovalov, D. G. Cocks and R. D. White, "Unified solution of the Boltzmann equation for electron and ion velocity distribution functions and transport coefficients in weakly ionized plasmas," *The European Physics Journal D*, vol. 71, p. 258, 2017.

[44] R. D. White, "Mass effects of light ion swarms in ac electric fields," *Physical Review E*, vol. 64, p. 056409, 2001.

[45] O. Sasic, J. Jovanovic, Z. L. Petrovic, J. de Urquijo, J. R. Castrejon_Pita, J. L. Hernandez-Avila and E. Basurto, "Electron drift velocities in mixtures of helium and xenon and experimental verification of corrections to Blanc's law," *Physical review E*, vol. 71, p. 046408, 2005.

[46] E. L. Patrick, M. L. Andrews and A. Garscadden, "Electron drift velocities in xenon and xenon-nitrogen gas mixtures," *Appl. Phys. Lett.*, vol. 59, no. 25, pp. 3239-3240, 1991.

[47] T. Makabe and T. Mori, "Experimental and theoretical analysis of the electron energy distribution functions in Townsend discharges in xenon," *J.Phys.B: Atom. Molec. Phys.*, vol. 11, p. 3785, 1978.

[48] H. L. Brooks, M. C. Cornell, J. Fletcher, I. M. Littlewood and K. J. Nygaard, "Electron drift velocities in xenon," *J.Phys.D: Appl. Phys.*, vol. 15, p. L51, 1982.

[49] A. K. Bhattacharya, "Measurement of breakdown potentials and Townsend ionization coefficients for the Penning mixtures of neon and xenon," *Physical review A,* vol. 13, p. 1219, 1976.

[50] L. Jacques, W. Bruynooghe, R. Boucique and W. Wieme, "Experimental determination of the primary and secondary ionisation coefficients in krypton and xenon," *J.Phys.D: Appl.Phys,* vol. 19, p. 1731, 1986.

[51] L. T. Specht, S. A. Lawton and T. A. DeTemple, "Electron ionization and excitation coefficients for argon, krypton, and xenon in the low E/N region," *J. Appl. Phys.,* vol. 51, no. 1, pp. 166-170, 1980.

[52] "LXCat, LAPLACE database, (measurements after 1975)," [Online]. Available: http://www.lxcat.net. [Accessed 18 July 2018].

[53] R. E. Robson, "Transport Phenomena in the Presence of Reactions: Definition and Measurement of Transport Coefficients," *Australian J. Physics,* vol. 44, pp. 685-692, 1991.

[54] R. E. Robson and K. F. Ness, "Velocity distribution function and transport coefficients of electron swarms in gases: Spherical-harmonics decomposition of Boltzmann's equation," *Physical Review A,* vol. 33, pp. 2068-2077, 1986.

[55] K. Kumar, H. R. Skullerud and R. E. Robson, "Kinetic theory of charged particle swarms in neutral gases," *Australian J. Physics,* vol. 33, p. 343, 1980.

[56] J. L. Pack, R. E. Voshall, A. V. Phelps and L. E. Kline, "Longitudinal electron diffusion coefficients in gases: Noble gases," *J. Appl. Phys.,* vol. 71, p. 5363, 1992.

[57] D. R. A. McMahon and B. Shizgal, "Hot-electron zero-field mobility and diffusion in rare-gas moderators," *Phsical Review A,* vol. 31, no. 3, pp. 1894-1905, 1985.

[58] B. E. Cherrington, Gaseous Electronics and Gas Lasers, Oxford: Pergamon Press, 1979.

[59] J. Wilhelm and R. Winkler, "Progress in the kinetic description of non-stationary behaviour of the electron ensemble in non-isothermal plasmas," *Journal de Physique Colloques,* vol. 40, no. C7, pp. 251-267, 1979.

[60] M. Moselhy and K. H. Schoenbach, "Nanosecond pulse generators for microdischarge excimer lamps," in *Proc. 14th IEEE Int. Pulsed Power Conf.*, Dallas, TX, 2003.

[61] B. J. Lee, H. Rahaman, S. H. Nam, M. Iberler, J. Jacoby and K. Frank, "Excimer emission from pulsed microhollow cathode discharges in xenon," *Physics of Plasmas,* vol. 20, p. 123510, 2013.

[62] R. J. Carman, R. P. Mildren, B. K. Ward and D. M. Kane, "High-pressure (>1 bar) dielectric barrier discharge lamps generating short pulses of high-peak power vacuum ultraviolet radiation," *J.Phys.D: Appl.Phys.,* vol. 37, pp. 2399-2407, 2004.

[63] T. Huiskamp, F. J. C. M. Beckers, W. F. L. M. Hoeben, E. J. M. van Heesch and A. J. M. Pemen, "Matching a (sub)nanosecond pulse source to a corona plasma reactor," *Plasma Sources Sci. Technol.*, vol. 25, p. 054006, 2016.

[64] B. I. Davydov, "Uber Die Geschwindigkeitsverteilung Der Sich Im Elektrischen Felde Bewegenden Elektronen," *Phys. Z. Sowj. Un.*, vol. 8, p. 59, 1935.

[65] C. S. Wang-Chang, G. E. Uhlenbeck and J. deBoer, Studies in Statistical Mechanics, vol. volume II, New York: Wiley, 1964, p. 241.

[66] F. Sigeneger and R. Winkler, "On the Mechanisms of Spatial Electron Relaxation in Nonisothermal Plasmas," *Plasma Chemistry and Plasma Processing,* vol. 17, no. 3, 1997.

[67] K. F. Ness and R. E. Robson, "Velocity distribution function and transport coefficients of electron swarms in gases. II. Moment equations and applications," *Physical Review A,* vol. 34, p. 2185, 1986.